Exploring the Earth

NORSAR Scientific Report No.2-2014

Semiannual Technical Summary

1 July – 31 December 2014

Tormod Kværna (Ed.)

Kjeller, August 2015

NORSAR

6.2 The DPEP Long-Period Detector for the NOA Broadband Array

6.2.1 Introduction

Since the NOA array upgrade to broadband sensors on all 42 sites in 2012, no automatic procedure was operating at NORSAR to analyze the new long-period part of the data. A long-period detector is therefore designed for near real-time, automatic detection focusing on teleseismic long-period surface-wave signals, specifically Rayleigh waves, using the broadband data from all 42 vertical sensors of the array.

Surface waves consist of Raleigh and Love waves, which can be recorded on horizontally and vertically oriented seismic sensors. Horizontal components are usually recording a mixture of Rayleigh and Love waves, which have different propagation characteristics. The detector searches for Rayleigh waves only, as these signals are easier to detect than Love waves. It is possible to isolate Rayleigh from Love waves by using vertical-component recordings only. This also allows exploiting the full beamforming power using all 42 vertical channels of the NOA array. Because of the large aperture of the NOA array, we focus on processing of teleseismic / far regional events where plane-wave approximation of the arriving wavefronts is valid.

Surface waves are dispersive, which means that their propagation velocity is frequency dependent. The goal of the developed detection routine is to detect the different portions of the incoming dispersive Rayleigh waves. To do that, the processing parameters had to be made frequency dependent. Real-time recognition of surface waves can be a significant improvement in nuclear explosion monitoring as well as a useful tool for earthquake seismology and noise analysis. A major issue is the differentiation between microseismic noise and seismic surface wave signals, as the polarization characteristics of these two signal types are of the same kind (Rayleigh waves) and their frequency and velocity contents are also very similar.

The new array processing algorithm for long-period data at NORSAR consists of two steps:

1. Detection Processing (DP).
2. Signal Attribute Processing (SAP).

These steps have been implemented by extensions to the NORSAR DP/EP program systems (Fyen 1987, 1989). Detection Processing (DP) consists of an STA/LTA detection and beamforming procedure. The STA/LTA detection processing parameters were found to be frequency dependent and were set for optimized triggering of the dispersive Rayleigh wavetrains. The steering parameters of the beam with the highest signal-to-noise ratio (SNR) are used as initial estimates of the apparent velocity and backazimuth (BAZ) of the detected signal.

During the Signal Attribute Processing (SAP) the detection parameters are refined. Onset time analysis is performed to find the best phase onset of the triggering signal and to estimate its dominant period, while a broadband frequency-wavenumber (f-k) analysis of the filtered data estimates its apparent velocity and backazimuth (BAZ). After beamforming with the SAP-estimated apparent velocity and BAZ values, the signal amplitude is measured and the onset time and dominant period are again recalculated.

To validate the results of the new processing algorithm, the detected Rayleigh-wave phases have been associated to and compared with seismic events reported in CTBTO's International Data Centre (IDC) Reviewed Event Bulletin (REB).

6.2.2 DP

The main goal of the Detection Processing is to detect the incoming dispersive Rayleigh waves using different frequency bands. In order to take account for the dispersion of surface waves, the array beams processed by the detector are constructed using multiple bandpass filter – propagation velocity combinations.

6.2.2.1 Frequencies

To reduce computing time, the original 40 Hz raw data are low-pass filtered and decimated to 1 Hz, yielding a Nyquist frequency of 0.5 Hz.

By assuming a minimum propagation velocity of 3.1 km/s of the arriving signals, the large-aperture geometry of the NOA array provide correct, spatially un-aliased sampling of signals up to a period of 40 seconds. For signals with higher propagation velocities this limit can be reasonably well extended to 50 second periods.

At very low frequencies, man-made noise has little influence on seismic recordings. The main noise sources at NOA in the long-period data are primary (6 – 8 s) and secondary (12 – 16 s) ocean microseisms. These are often referred to as “ocean noise”, and are often pronounced at the NOA array, which is located only $\sim$ 200 km from the North Atlantic Ocean. Atmospheric low pressure systems are regularly observed in the North Atlantic, and are very strong sources of microseisms. The dominant BAZ at NOA of these signals varies between 225° and 345° and thus also coincident with parts of the seismicity in the Pacific Ocean region. These BAZ values, previously observed by e.g., Köhler et al. (2011), have been also confirmed during the detector testing. Since microseisms have the form and particle motions of propagating Rayleigh waves (Haubrich et al., 1963, Longuet-Higgins, 1950) and are very coherent among the different traces (see Figure 6.2.1), ocean noise can lead to incorrect classification of Rayleigh wave signals from earthquakes. Secondary microseisms have, as mentioned above, typical periods of 12 – 16 s. This means that these kind of microseisms are broadly overlapping in the period range with the shorter surface-wave periods of about 10 – 20 s. Since empirical tests on the available data showed that teleseismic Rayleigh waves recorded at NOA have little energy at shorter periods, the DPEP LP detector analyzes data in the 10 – 50 s period range to avoid both aliasing and the influence of primary microseisms.

6.2.2.2 Dispersion curves

For the DPEP LP Detector, the dispersion curves computed by Köhler et al. (2012) are used as reference for the expected dispersion behavior of Rayleigh waves. For each NOA subarray, Köhler et al. (2012) report phase- and group-velocity dispersion curves in the 3 – 70 s period range. Since differences among the NOA subarrays are small, a single set of filter – velocity combinations samples the whole set of dispersion curves. Numerous real-data tests show a clear correlation between the reference phase-velocity curve and the observed frequency-depending propagation velocities estimated by f-k analysis on the triggered signals. Therefore, the applied filter-velocity combinations used by the DPEP LP Detector (Table 6.2.1) are based on the Rayleigh wave phase-velocity curves.

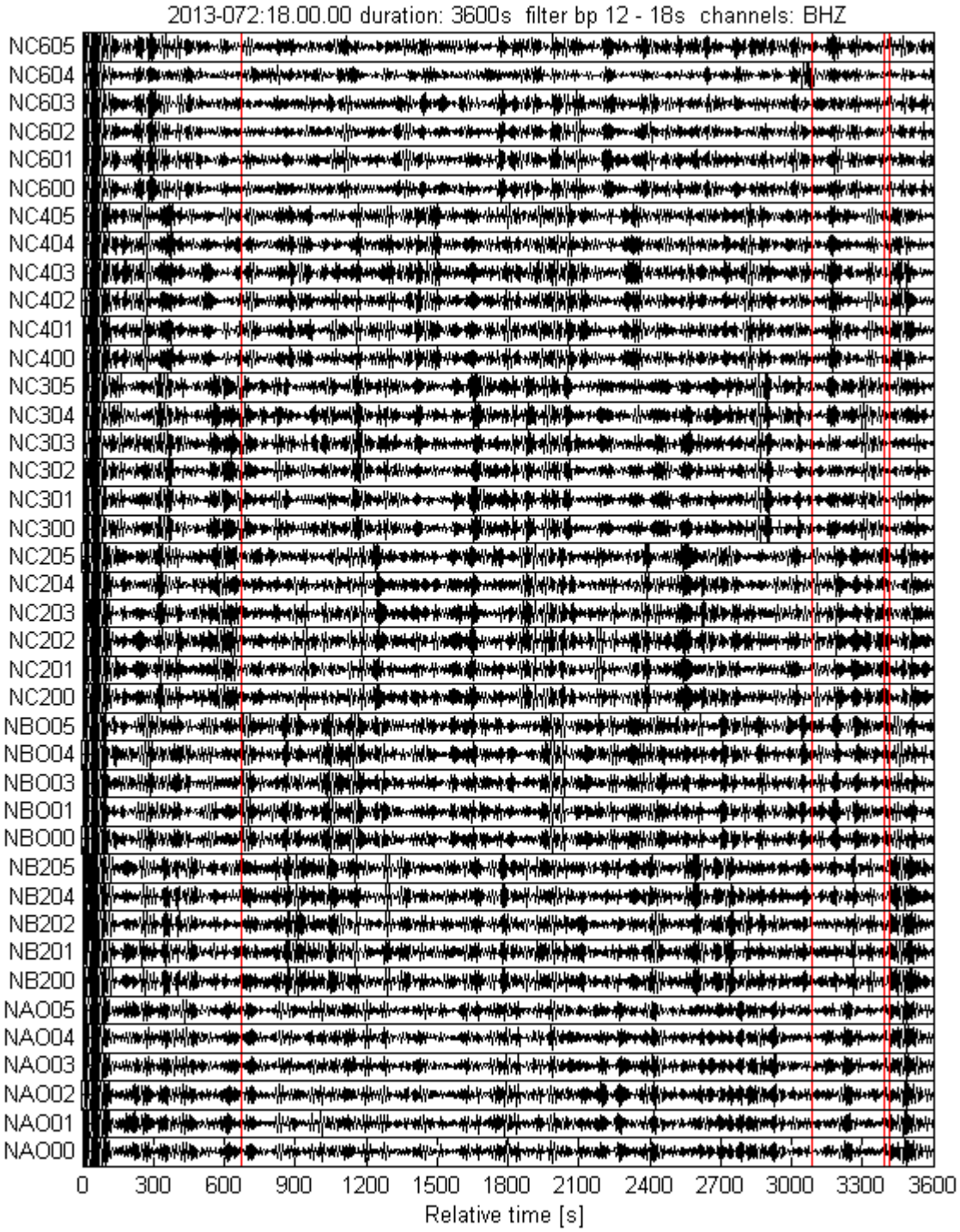

Fig. 6.2.1 Trace stack for 41 available (out of in total 42 total) vertical channels, showing records of 13 March 2013 at 18.00 in the 0.02 – 0.1 Hz frequency band. Most of the visible signals are due to ocean microseisms, whose coherency can be seen among the traces. The red lines are microseism-triggered signals. At the beginning of the record, a filtering artifact can be observed.

6.2.2.3 Filter – velocity combinations

The filter-velocity combinations are set to sample the chosen reference-phase-velocity dispersion curves. To reduce the influence of the secondary ocean microseisms we use filters with a relatively wide bandwidth. A set of six filters covers the period range of interest (10 – 50 s), where the lower frequency of each filter is always half of the upper frequency limit (Table 6.2.1). The geometrical progression of the filter bandwidths provides a sufficiently large bandwidth to reduce the detector sensitivity in the noisy 10 – 20 s range, and also prevents any monochromatic signal oscillations to be present in any filter band. The order of the Butterworth filters is set to the standard value of 3 to avoid ringing artifacts.

Table 6.2.1 Ranges (F1 – F2 Hz or T1 – T2 s) of the chosen Butterworth bandpass filters, their middle periods and the corresponding phase velocity used for beamforming.

f1 [Hz]	f2 [Hz]	T1 [s]	T2 [s]	Mid T[s]	Phase Velocity [km/s]
0.05	0.1	20	10	15	3.4
0.04	0.08	25	12.5	18.25	3.5
0.033	0.066	30	15	22.5	3.6
0.028	0.057	35	17.5	26.25	3.7
0.025	0.05	40	20	30	3.8
0.020	0.04	50	25	25	3.9

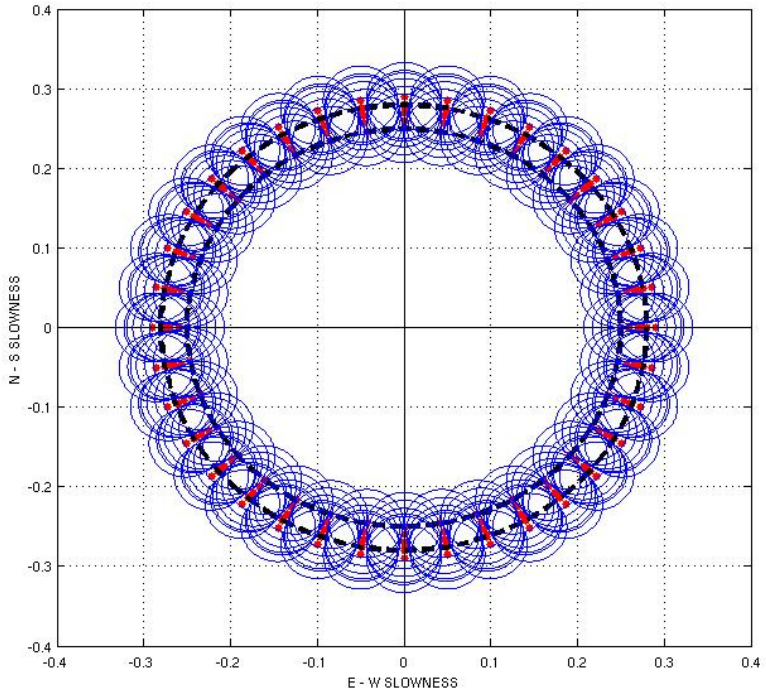

Fig. 6.2.2 Horizontal slowness plot displaying the set of steering parameters for the detection beams computed by the DPEP LP Detector. Red points show the beam steering points and the surrounding circles represent a radius of 10 degrees. The black dotted lines show reference velocity/slowness values of 3.5 and 3.9 km/s for surface waves.

6.2.2.4 Beamforming

The DPEP LP Detector computes a set of multiple beams at selected BAZ intervals, using the six different filter-velocity combinations listed in Table 6.2.1. Figure 6.2.2 shows the coverage in slowness space of the different detection beams. Empirical tests demonstrated that a 10° BAZ sampling yields good resolution in terms of recognizing the true seismic wave source direction (see Figure 6.2.3.

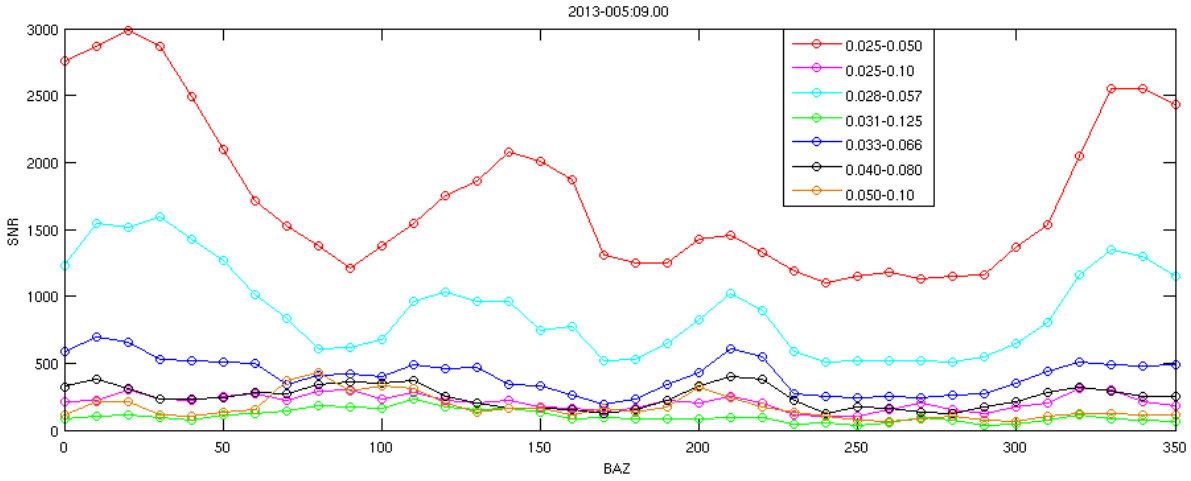

Fig. 6.2.3 The curves are showing the SNR of the detections found on all 216 beams computed in a time window including only the P-wave arrival of the 5 January 2013 08:58, Mw 7.5 Alaska event. It is clearly possible to recognize the source BAZ from the SNR maxima. The theoretical BAZ of the arriving signal is ~0°. Different curves represent different bandpass filters, as shown in the figure legend.

6.2.2.5 STA/LTA detector

STA/LTA parameters test

After beamforming, an STA/LTA detection algorithm runs on each of the computed beams. This allows detecting and extracting apparent velocity and BAZ of the triggering signal in the different frequencies. The parameters of the STA/LTA algorithm are tuned to maximize SNR values for Rayleigh waves only, in order to obtain a “clean” Rayleigh wave observation list while reducing the number of noise triggers and body-wave detections. This can be achieved by setting most of the parameters to be frequency-dependent.

For more detailed information on the definition of the different used STA/LTA parameters see Schweitzer et al. (2011) and Trnkoczy (1999). In order to optimize the settings of the detection parameters STA length, LTA delay, STA delta, and the LTA update parameter SIGMA, we first investigated the detection SNR of signals from three teleseismic earthquakes with good long-period signal radiation (Bougainville region, Papua New Guinea, 19 April 2014 13:28, Mw 7.5; Offshore Tarapaca, Chile, 1 April 2014 23:46, Mw 8.1 ; Vancouver Island, Canada, 24 April 2014 03:10, Mw 6.5).

The SNR has been investigated by systematically changing the STA length from 1/f1 to 1/f2, the LTA delay from 1/f2 to a maximum of 500s and of SIGMA from 4 to 8, where f1 and f2 refer to the higher and lower corner frequency of the Butterworth bandpass filters (see Table 6.2.1). The highest SNR is found for an STA length of 1/f2 s and an STA up-date interval delta of 1.0 s.

The results obtained with these values produce a very rugged SNR trace with several peaks, leading to a large number of triggers. The best compromise between resolution and non-redundant information has been achieved by smoothing the SNR trace by changing STA length and STA delta values to 2/f2 s and 2.0 s, respectively. The SNR loss caused by the smoothing is low and acceptable; as it affects mostly unwanted high SNR body wave phases (see Figure 6.2.4).

In the final implementation, the triggering SNR threshold is set to 4.5, the LTA delay to *4/f2* s and LTA smoothing parameter SIGMA to 5 (see Figure 6.2.5).

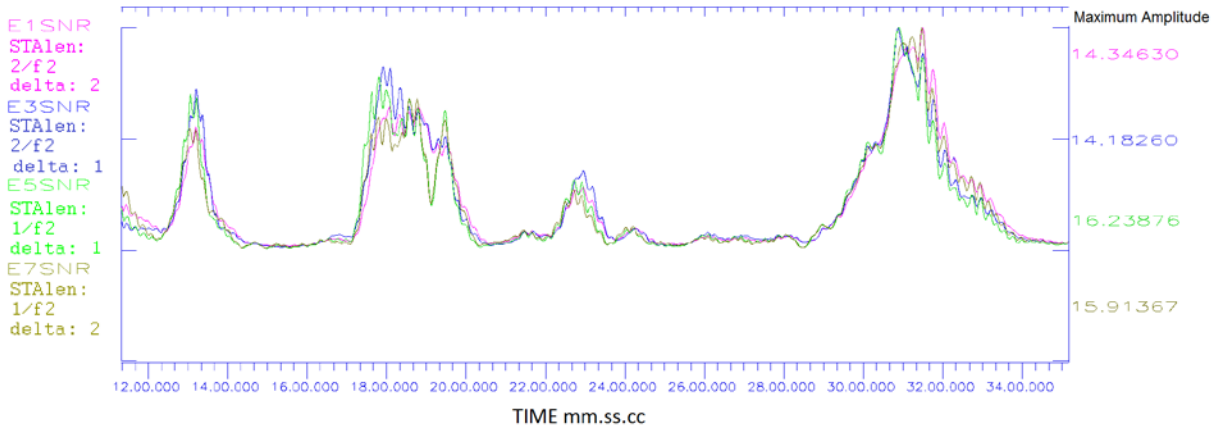

Fig. 6.2.4 SNR trace for later body waves and Rayleigh waves arrivals from the 5 January 2013 08:58, Mw 7.5 Alaska event. Each trace is calculated using different STA length and STA delta values. The trace names with the processing parameters are shown to the left.

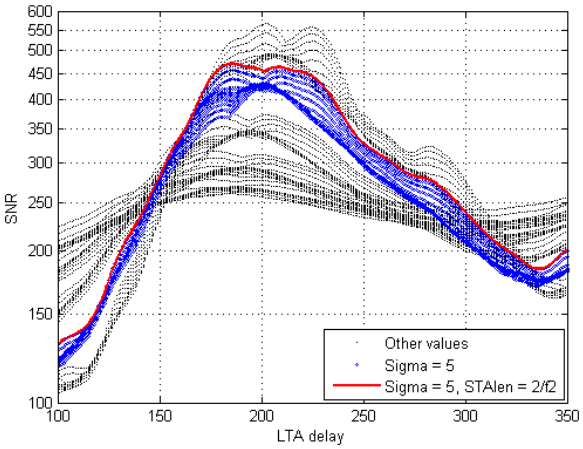

Fig. 6.2.5 Relationship between LTA delay and max SNR for data from the 19 April 2014 13:28, Mw 7.5 Papua New Guinea event. The max SNR for the Rayleigh-wave package is shown for all tested sigma, STA length and LTA delay values. Blue dots are computed with a sigma value of 5, while the red line is computed using the sigma-STA length combinations later implemented in the near-real time processing at NORSAR.

Reading and detecting

The detection processing employs the aforementioned STA/LTA parameters. To reduce the number of triggers within each signal, a detection reduction algorithm is running on each filtered beam. The procedure is summarized as follows, where *T* is the central period of the filter bands (see Table 6.2.1):

Triggers within a time window of 3*T are grouped as one detection

After a time period of 4*T, triggers are seen as part of a new signal.

The dependency on the different frequencies of the filters (and thus to an average period of the expected signal) allows the algorithm to merge triggers coming from high frequency SNR oscillations, while at the same time setting a reasonable limit to time-separate lower frequency signals.

After detection reduction, the detections are reported in an ASCII file (DPX file). For each group of triggered beams, only the parameters of the beam with the highest SNR are listed.

6.2.3 The signal attribute processing (SAP)

The DPX detection lists are then used as input for the parameters refinement operated in the SAP.

6.2.3.1 Onset time estimation

This part of the processing follows the original structure of the RONAPP processing package (Mykkeltveit and Bungum, 1984). Onset time estimation acts on each detection and is tuned to be dependent on the corner frequencies of the filters applied to the beams. The algorithm backtracks in time starting from the detection time, which is the time at which the signal exceeds the SNR threshold. This is usually quite different from the true signal onset time. The onset estimation process also estimates the signal period, which is fundamental to fine-tune the later processing related to the expected signal dispersion. Three parameters are set to stop the backtracking:

1) Maximum length of backtracking in [s]: **4*T1.** T1 is the longest period of the filter cutoff (see Table 6.2.1)

2) Minimum ratio (*first cycle amplitude / RMS noise level)*: **2.0**

3) Minimum ratio (*first cycle amplitude / maximum signal amplitude)*: **0.6**

The noise RMS is calculated in a time window starting *(T1 + T2)* before the detection time and backtracking by (*3 * T1)*. The maximum amplitude search is made in a *+/- T1* long time window around the detection time.

6.2.3.2 F-k analysis

Following the first onset time estimation, broadband f-k analysis (Kvaerna and Doornbos, 1986) is applied to the analyzed signal. The length of the time window is set to be frequency dependent. The length of the time window *t* should include at least a few periods of the signal (in our case ~6) and sample the slowest propagating frequency component. The window length is thus set to $t = a*T + d$, where *T* is the signal period estimated by preceding onset analysis. *a* is a user-defined constant which is set to larger values for the slow velocities typical of Rayleigh waves. *a* is introduced to take into account the longer duration of surface-wave signals, which travel with a lower velocity than S-waves. The *d* value is the minimum duration of the time window, which is set according to the slowness resolution of the array.

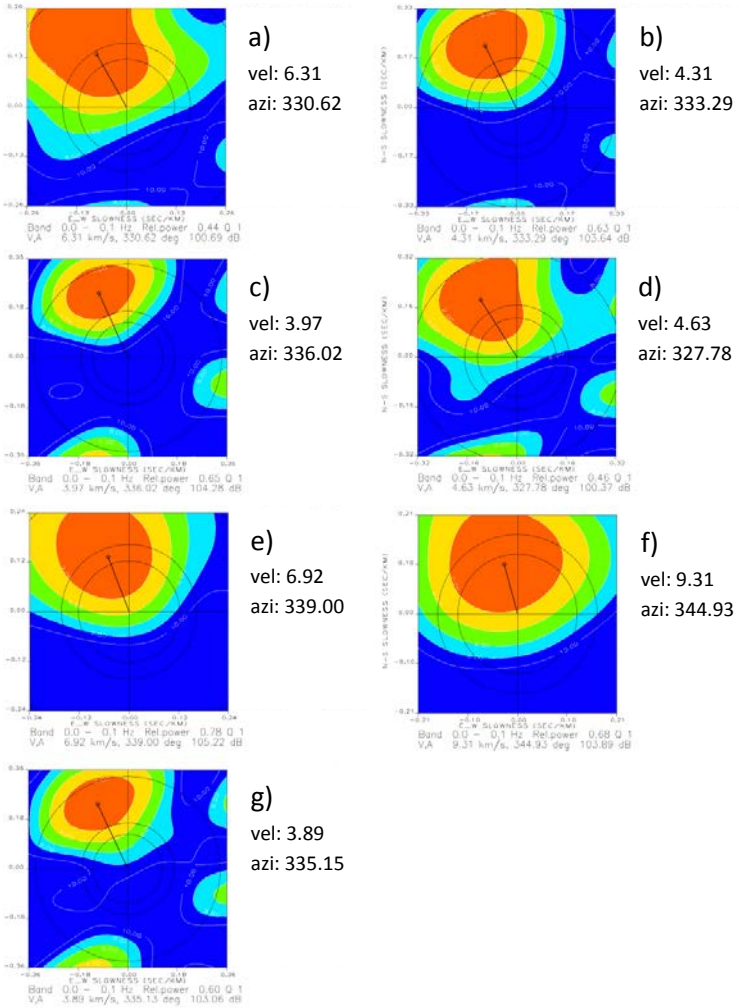

Fig. 6.2.6 Broadband f-k spectra computed in the different time windows for a single triggered phase of the 5 January 2013 08:58, Mw 7.5 Alaska earthquake:
***a**) Centered at the onset time from the onset estimation procedure; **b**) centered at the detection time; **c**) centered 2 x T1 after the detection time; **d**) centered 2 x T1 before the detection time; **e**) centered at the detection time with a window length of T1; **f**) centered at the onset time with half-long time window; **g**) centered at the onset time with 1.5 x long time window.*

The broadband f-k analysis is applied to a set of 7 to 8 different time windows having different start and end times, different durations, and centered either on the detection (trigger) time or the estimated onset time. The f-k analysis results from these different choices can differ significantly (see Figure 6.2.6). The apparent velocity and BAZ estimated in the time window having the highest value of (SNR * f-k power) is reported from the f-k analysis.

6.2.3.3 The f-k beam

A new beam is calculated using the velocity and BAZ reported from the f-k analysis. On this so-called f-k beam, a second search for the onset is made, using the same procedure as described in section 6.2.3.1. The SNR of the detection is also reestimated on the f-k beam using the reestimated onset time. Due to local noise and scattering of the long-period seismic energy, several detection beams with quite different BAZ values can exceed the SNR threshold, and the BAZ value of the detection beam with the highest SNR may not correspond to the "true" BAZ of the arriving signal. However, the beams calculated after fk-analysis ("f-k beams") show major differences if compared to the beams computed by the DP processing before the f-k analysis. For the f-k beams the SNR of seismic noise detections is lowered, and the consistency of the BAZ estimates for each event is much more stable than for the BAZ reported by the initial detector (DP), as shown in Figures 6.2.7 and 6.2.8. This improvement is due to optimizing the analysis window (onset time estimation) and the denser slowness gridding of the fk-analysis, as compared with the DP beam gridding shown in Figure 6.2.2.

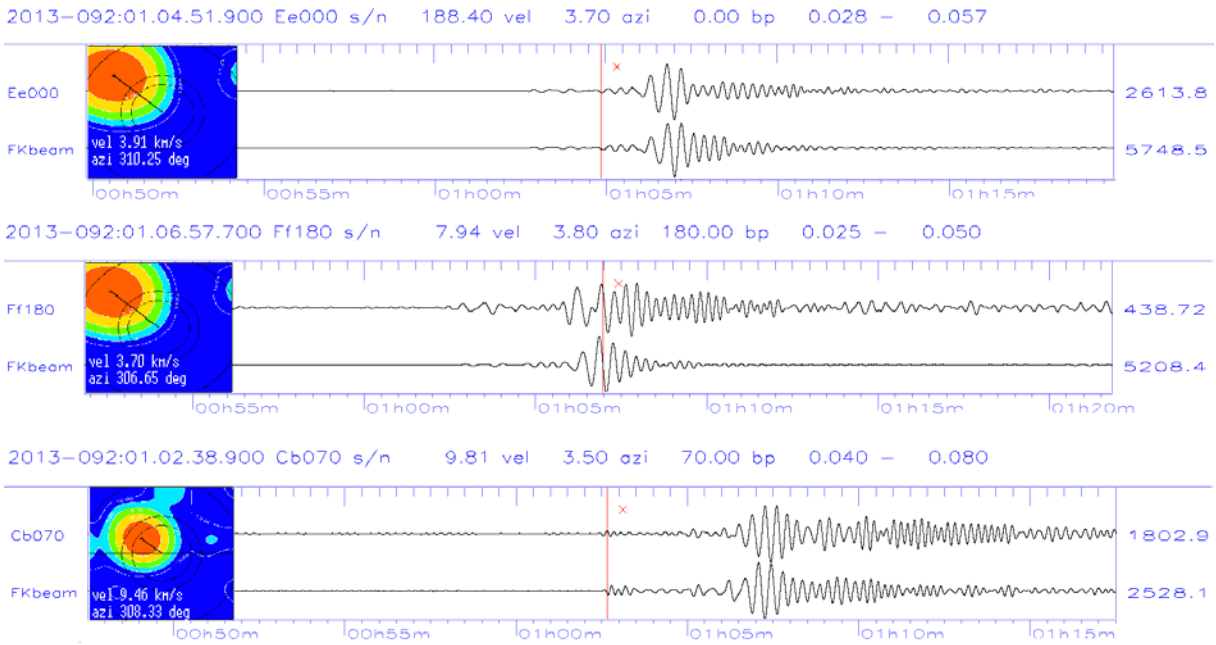

Fig. 6.2.7 Icelandic region event on 2 April 2013 00:59 recorded at NOA, showing three different detections within the wavetrain. The detection times are marked by red vertical lines. Each panel shows the detection beam (top) and the f-k beam (bottom). The parameters shown above each panel of beams refer to the detection-beam parameters. The f-k analysis results are plotted together with the corresponding apparent velocity and BAZ values. The detection beam BAZ ("azi" values on top of each panel) shows noticeable instability, whereas the back-azimuth values shown in the f-k plots are very consistent.

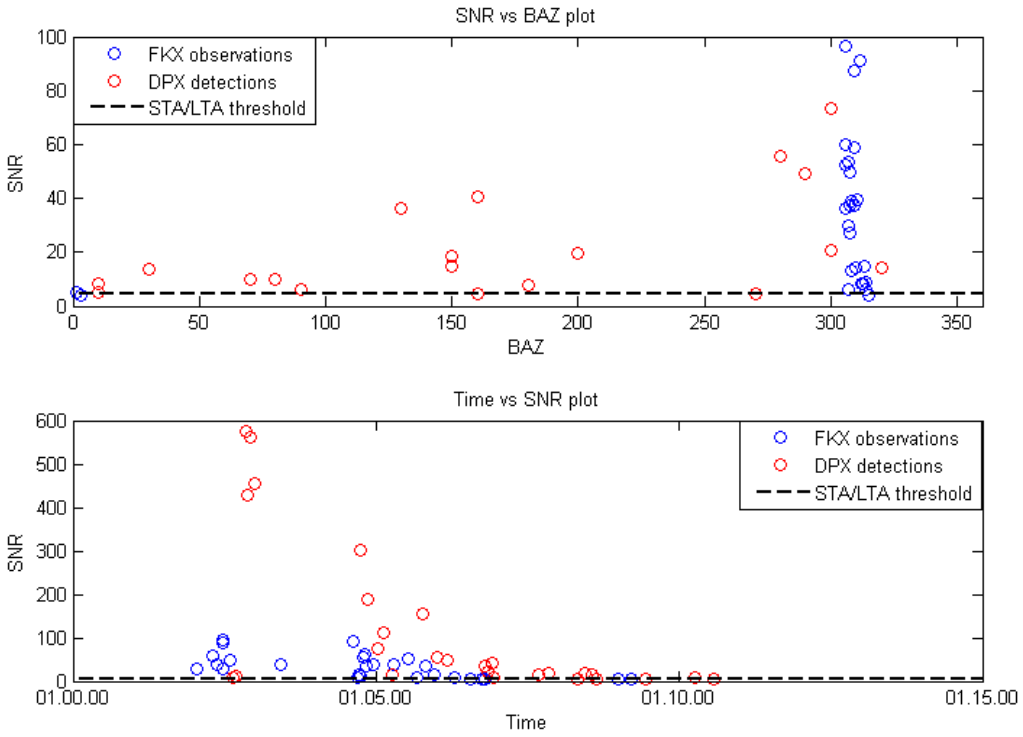

Fig. 6.2.8 Plot showing the differences between detection beam parameters (red) and signal parameters from f-k analysis (blue) for the 2 April 2013 00:59 Icelandic Region event (see also Figure 6.2.7). On top panel the SNR is plotted against the BAZ, while on bottom panel the SNR is plotting as function of time. The dotted line represents the SNR threshold level of 4.5. It is clear that the results of the f-k analysis improve the SNR and cluster at and azimuth close to the theoretical value of 305°.

6.2.3.4 Phase identification

The phase identification procedure is based on velocity estimates reported from the f-k analysis. As seismic arrays are capable of extracting velocity and period of the recorded waves, the phase naming criteria for Rayleigh waves are based on the signal's phase velocities and dominant period. All onsets with either an observed phase velocity between 3.1 and 4.5 km/s or an observed dominant period larger than 35 s are identified as LR (Rayleigh wave) by the algorithm.

By comparing the results of analyst reviewed phase recognition of the observations with the results of the automated processing for the time between 1 and 9 January 2013 it is possible to evaluate the quality of the automatic phase identification criteria (Figure 6.2.9). The automatic phase naming seems to separate reasonably well body- and surface wave detections, but fails in separating the LR observations from triggers by the secondary ocean microseisms because of their overlap in both the frequency and the velocity ranges (see Figure 6.2.9, bottom)

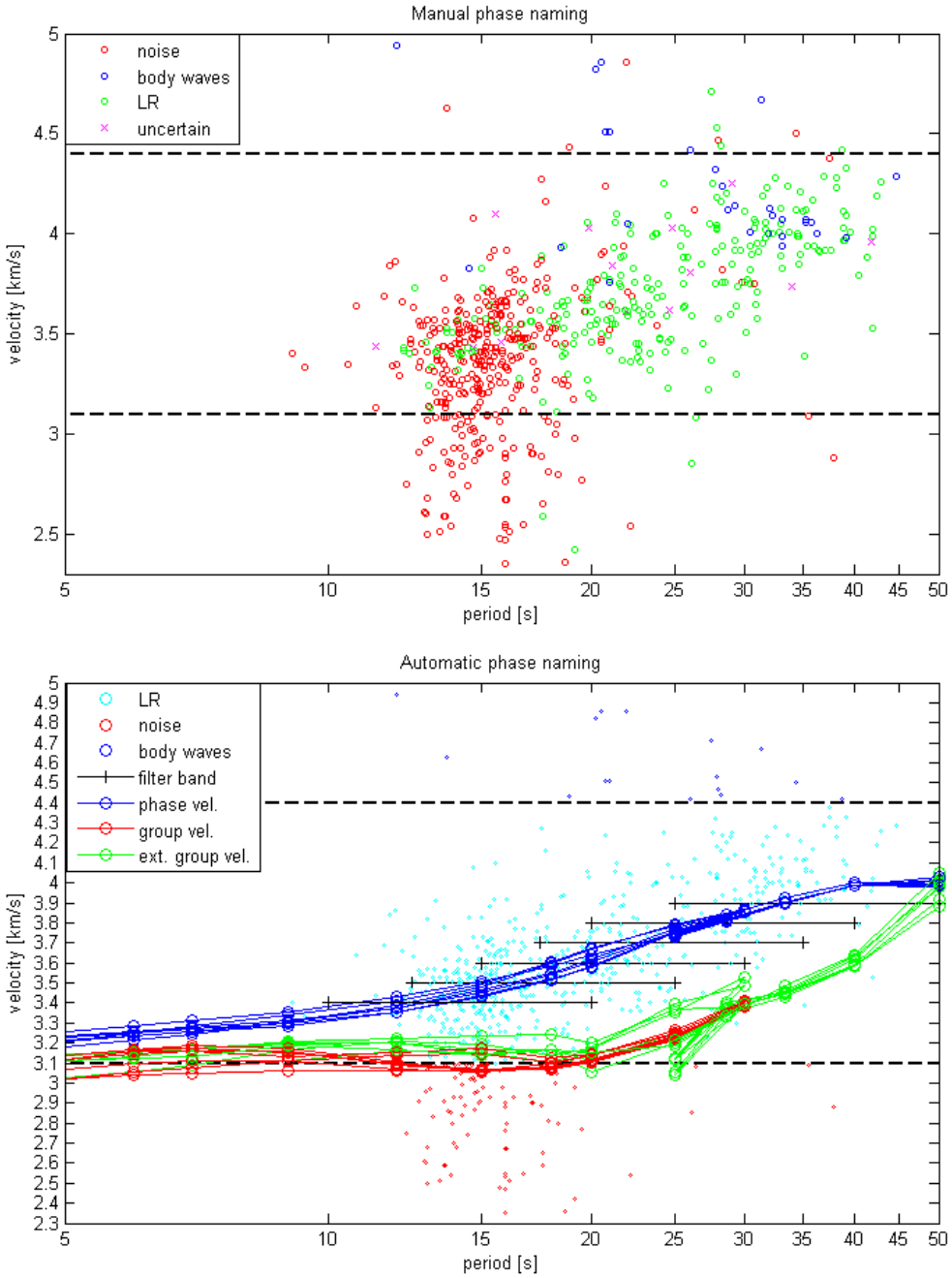

Fig. 6.2.9: The top panel shows the manual phase naming of the detections recorded between 1 and 9 January 2013. Noise detections are displayed in red, Rayleigh waves in green and body waves in blue. A cross marks unclear cases. It is possible to visually identify the critical areas in which the dispersive Rayleigh wave detections overlap with the noise observations and with the slowest propagating body waves.
At the bottom panel the automatic analysis results for the same time interval are shown. The dashed lines in both panels show the chosen velocity constraints to define LR waves. Cyan symbols within the velocity limits are assumed to represent LR arrivals, red are noise, and blue are body waves. The blue, red and green lines represent respectively the dispersion curves for phase-, group- and extended group velocities at the 7 NOA subarrays as reported by Köhler et al. (2012).

6.2.3.5 Recognizing the disperse character of surface waves

To improve the phase identification, further analysis on selected known events was performed. Of particular interest is the detector's ability to recognize surface-wave energy in the different frequency bands (see Figure 6.2.10).

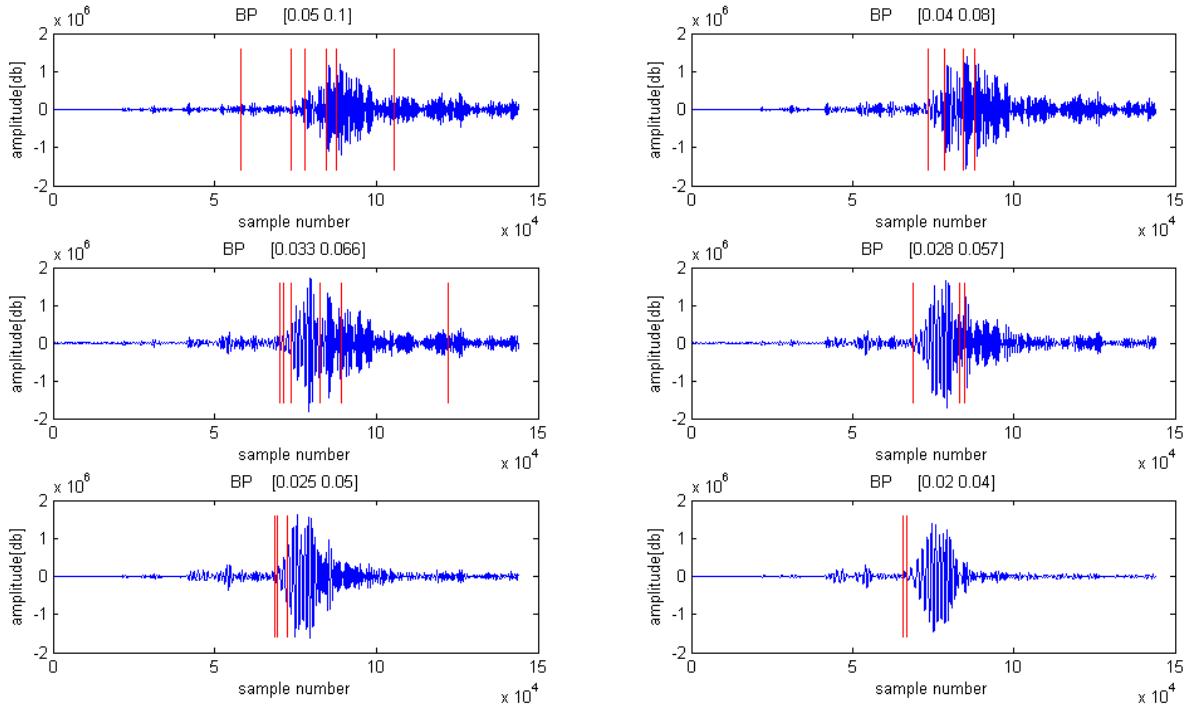

Fig. 6.2.10 Plots of automatic detections (red lines) in different frequency bands for the 05 January 2013 09:00 Alaska earthquake. Each seismogram shows the filtered data (not beams) as recorded at array site NAO01. The passband of the Butterworth filter is given on top of each panel (in Hz).

By plotting the detector results on top of Amplitude Spectral Density (ASD) plots for the 5 January 2013, 09:00 Ms 7.6 Alaska event, it is possible to evaluate the LR observations and how they show the dispersive behavior of the Rayleigh wavetrain both in time and frequency. Figure 6.2.11 shows such plots as a stack of all ASDs calculated for all 5 sites of the NB2 subarray of NOA. In addition are shown the onset time and frequency range of the corresponding DPX detections (upper panel), and the onset time and frequency range from the SAP processing. Note that the ASDs of the individual sensors were not phase delayed during the stacking as this would amplify only one specific phase velocity. It is clear that all major seismic onsets of the record were detected with the chosen set of detection beams.

For large events for which the detector create several triggers within the wavetrain, it is also possible to recognize and reconstruct the Rayleigh-wave dispersion curves by plotting the estimated signal period and corresponding velocity values as a function of time (see Figure 6.2.12).

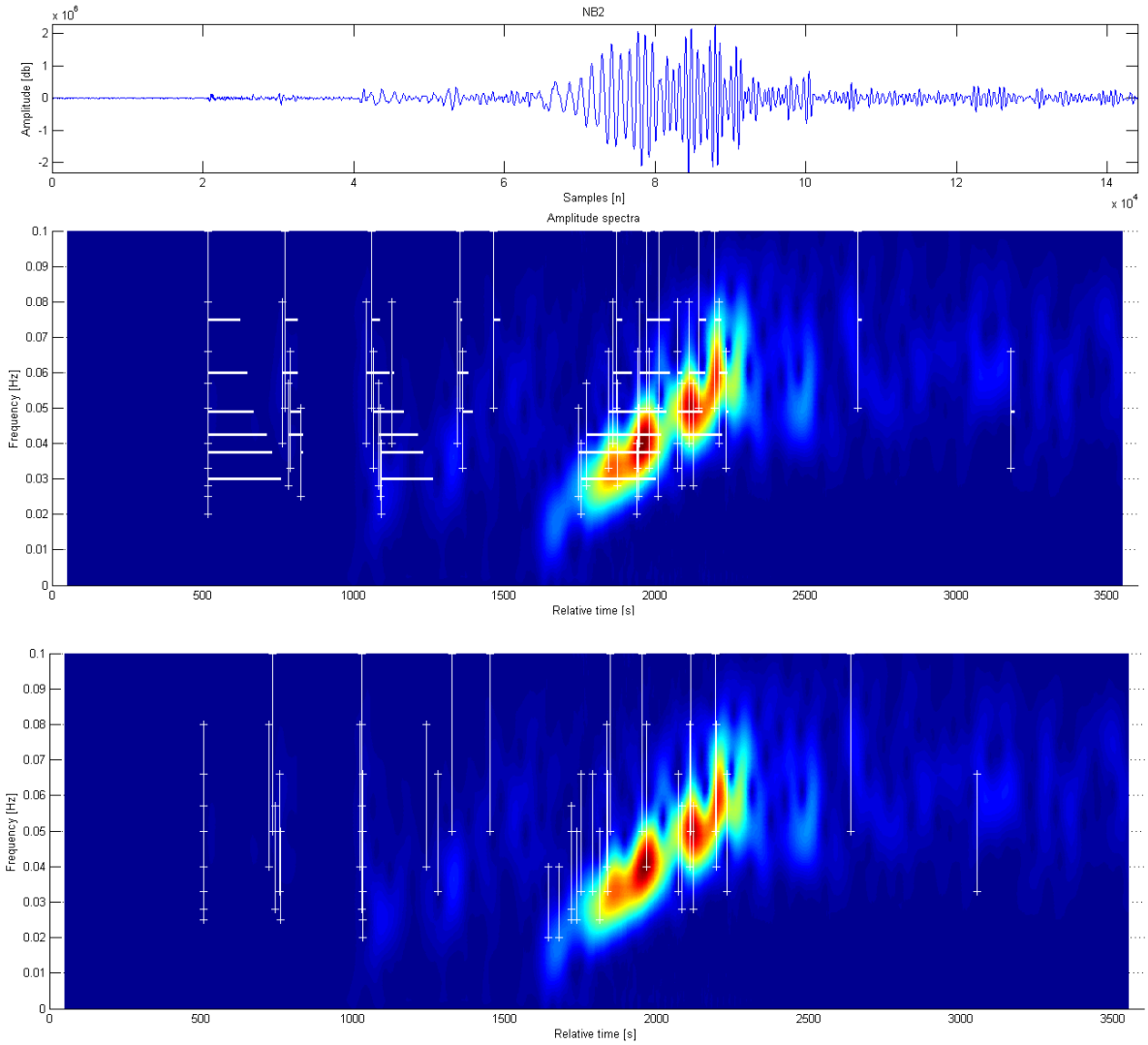

Fig. 6.2.11 TOP panel: stacked ASD for the 5 January 2013 09:00 Alaska event as recorded at subarray NB2. The vertical lines represent the DP detections as from the DP, with their length indicating the frequency range of the different triggers. The horizontal lines represent the time windows for which the detector is in triggering mode.
BOTTOM panel: ASD plot of the same event, with the vertical lines representing the onset time and frequency range of the phases as recognized by the SAP.

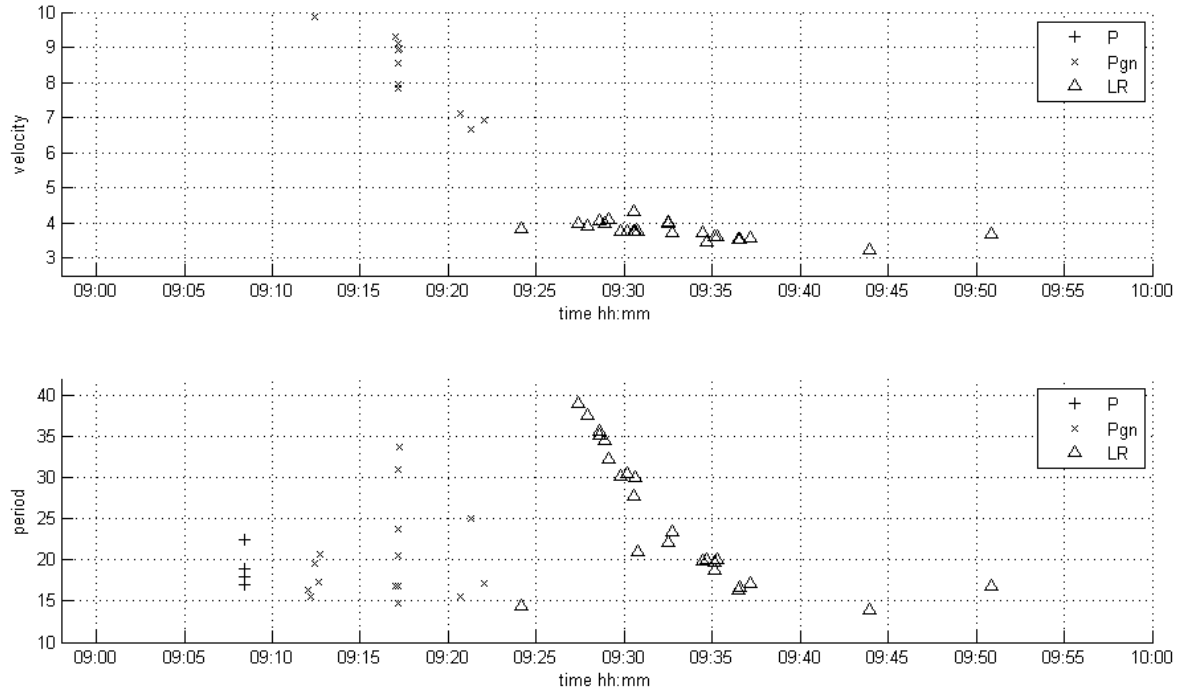

Fig. 6.2.12 The top panel shows the automatically estimated velocities from the f-k analysis plotted against time for the 5 January 2013 09:00 Alaska event. The lower panel shows the estimated dominant signal periods plotted as function of time. The theoretically expected decrease in signal period of the dispersive wavetrain can be clearly observed for the LR arrival, while P and other types of body-wave signals (Pgn/S) at 09:08 and 09:17 do not show any dispersive character. For LR a corresponding slight decrease in measured phase velocities is observed (upper panel).

6.2.4 Detector event coverage

In order to validate the results achieved by the detector on the recorded two-year dataset, a Matlab event association program for Rayleigh wave observations was written. By associating the observed Rayleigh waves to verified events we can estimate the capability (or "event coverage") of the new DPEP LP Detector to detect Rayleigh waves.

6.2.4.1 Associating Rayleigh wave observations to events in the IDC Reviewed Event Bulletin

As a reference we use reported Rayleigh waves (LR phases) in the IDC Reviewed Event Bulletin (REB). The results from the DPEP LP Detector (including f-k analysis) are compared to a selection of events from the REB which has a likelihood of producing "detectable" LR phases at NOA. Event selection criteria have been set up to select only events that could possibly produce surface waves, mainly avoiding very deep and small earthquakes and taking into account the higher detectability of closer events (40° from NOA) by including magnitude, depth and distance thresholds. Events are also included for which an LR phase detection is reported from any station of the International Monitoring System (IMS) or for which a body wave detection is reported from one of the North European arrays.

The event association program estimates for each listed event a possible Rayleigh-wave arrival time and a BAZ window, defining an "event box" to which each detection is compared. LR observations

with time and BAZ falling inside such an event box are considered as associated to that event (see Figure 6.2.13).

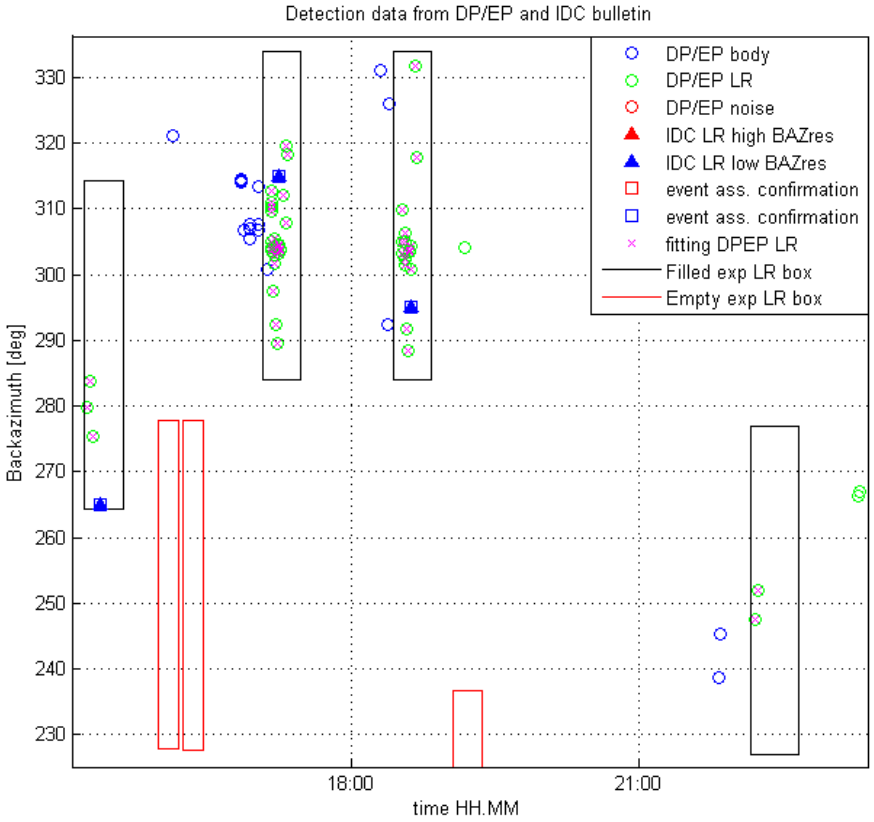

Fig. 6.2.13 Example of event boxes and the associated NOA surface wave detections both from the IDC (REBs) and the DPEP LP detector system.
Circles represent DPEP observations: blue - body waves, green – Rayleigh waves, and red - noise; associated LR detections are filled with a magenta cross.
Triangles are reported IDC (REBs) LR observations at NOA: red – LR with large BAZ residual, blue – LR with small BAZ residual. Event boxes are shown as rectangles: black if detected by the DPEP system, red if not.

A careful selection of minimum and maximum expected group velocities (2.8 and 4.1 km/s, respectively) for the definition of the expected arrival time window provided good automatic association results. The BAZ width of the event boxes is set to ±25° (see Figure 6.2.14).

The program also reassociates the LR observations detected by the IDC's own processing (see Stevens & McLaughlin (2001) when using NOA data (called IDC NOA LRs), allowing a comparison of the IDC long-period processing with the NORSAR DPEP LP Detector.

The IDC NOA LRs are included in the statistics only if the BAZ residual is smaller than 25°. This is because larger residuals mostly proved to be wrong associations. A large part of the wrongly associated LR phases have BAZ observations from the main noise directions between 225° and 345° (see Figure 6.2.14).

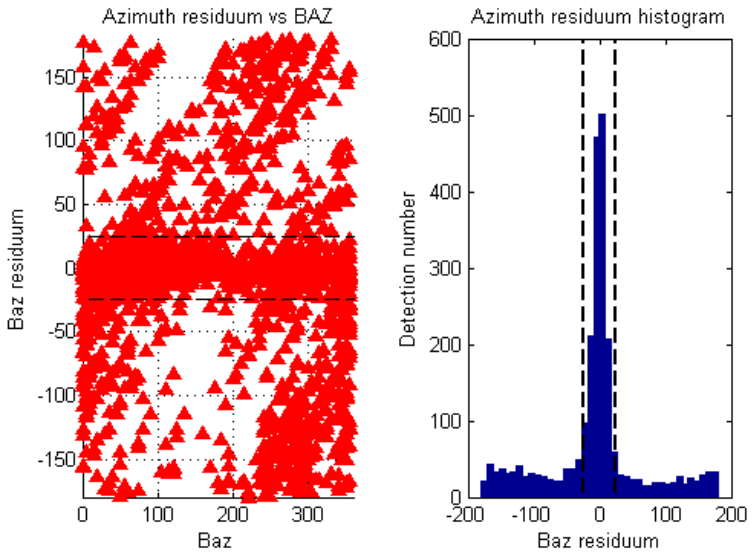

Fig. 6.2.14 BAZ residuals as reported in the REBs of the IDC. Left: BAZ vs. BAZ residual. Right: histogram of the same BAZ residuals. The dashed lines mark the ± 25° limits to define the event boxes in Figure 6.2.13.

6.2.4.2 Statistical analysis of event association results

This chapter presents the results of the statistical analysis over two years of available broadband data since the NOA recapitalization (31/08/2012 – 31/08/2014). From the event association results we have introduced several tests to evaluate the DPEP LP detector performance:

- Observe the amount of associated/non-associated LR detections and analyze their parameters to identify possible noise sources. As criteria were used all DPEP LR detections arriving within a time window defined by the group velocities between 2.8 and 4.1 km/s after the source time and which have a BAZ deviation of less than 25°.
- Observe the amount of events detected by the DPEP LP detector, the IDC detector, or both to compare their effectiveness using the same input data. Seismic events are defined as possibly detectable if they meet the conditions for event selection described in section 6.2.4.1.
- Analyze the capability of the new processing to detect events previously undetected by NOA as reported IDC REB.

The statistical analysis shows that using these criteria, 60% of the DPEP LR detections can potentially be associated with an event in the IDC REB, while the remaining 40% can be related to triggers due to ocean microseisms, to the detection of events excluded by the event selection process, or to seismic noise and instrumental noise.

Number of NOA LR detections from DPEP		
All DPEP detections	134950	100%
Associated to REB events	80189	60%
non-associated	54761	40%

Number of NOA LR detections from IDC		
All LR in REBs	4985	100%
With small BAZ residual	3043	61%
With large BAZ residual	1942	39%

"Detectable" REB events		
Total number of events	21760	100.0 %
Events without LR observation	15359	70.58 %
NOA events detected by IDC (with small BAZ residual) or DPEP	6401	29.4 %
NOA events detected by DPEP	5856	26.9 %
NOA events detected by IDC (with small BAZ residual)	3043	13.9 %
NOA events detected by DPEP only	3360	15.4 %
NOA events detected by IDC (with small BAZ residual) only	545	2.5 %
NOA events detected by both	2496	11.5 %
NOA events detected by IDC with large BAZ residual	1958	9.0 %

It is clear that the new processing scheme could provide a noticeable improvement in terms of event detection capabilities (see Figure 6.2.15). The proposed detector finds potential LR surface waves for 26.9% of the selected events from the IDC REB, while the IDC reports only for 13.9% of the events LR observations. Of the total number of events, 15.4% have potential DPEP LR detections and no IDC LR detection, while the amount of "missed" events, for which Rayleigh waves are detected by the IDC but not by the DPEP system, is only 2.5%. This percentage can be largely accounted by very dense seismic sequences otherwise correctly detected or in some cases the IDC association might be based on ocean microseism detections having by chance the correct BAZ. That this is a larger problem can be seen in Figure 6.2.16. Here observed BAZ values are plotted with respect to time. A band of non-associated LR detections is clearly visible when a low pressure system is located in the North-Atlantic.

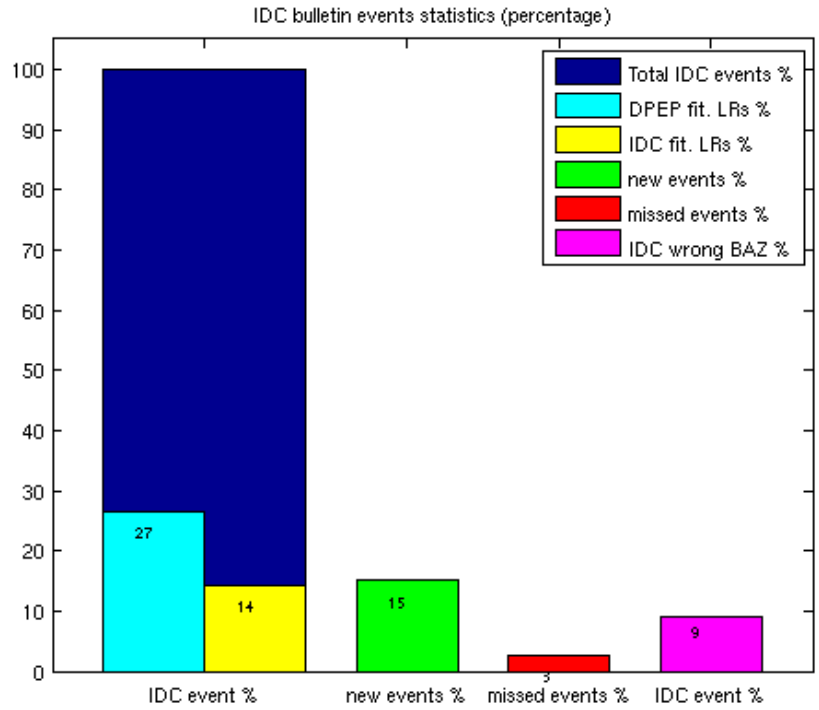

Fig. 6.2.15 IDC bulletin statistics for 2013. All the data are shown as % of the total selected events from the IDC REB.

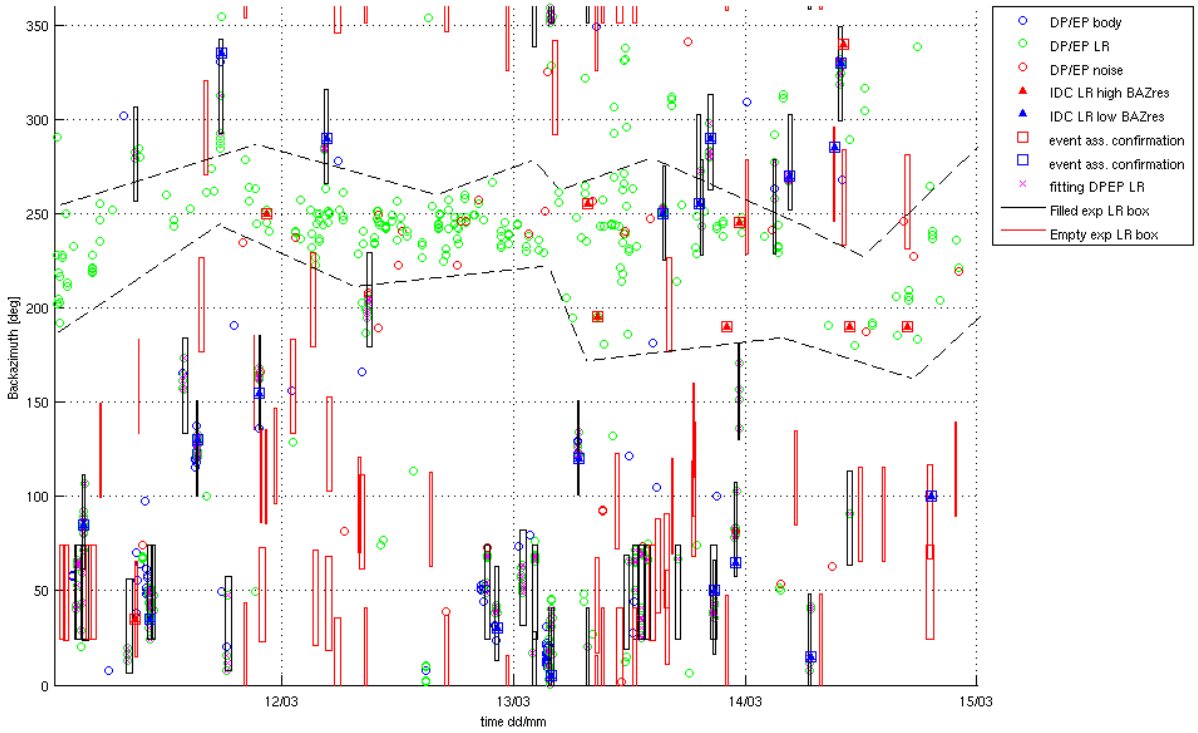

Fig. 6.2.16 Observed microseisms during a time window (11-15 March 2013) showing no major earthquakes. The clustering of unassociated DPEP LR (green circles) and IDC LR (red triangles within a square) observations in the contoured noise azimuthal area can be clearly seen.

The analysis of the surface-wave magnitudes Ms and Ms1 of the detected and undetected events also demonstrates that the new detector is able to observe LR phases for all major earthquakes (see Figure 6.2.17 and 6.2.18). The mean (median) of all surface magnitudes Ms and Ms1 is 3.8 (3.8) for the DPEP detected and 2.4 (3.1) for the DPEP undetected events.

The analysis of LRs detection parameters shows the noisy nature of most of the non-associated detections. The velocities, periods and BAZ are all displaying values that are typical for ocean microseisms, which have in the mean lower SNR, smaller periods, lower propagation velocities and less reliable f-k analysis results.

DPEP LRs extracted parameters for the year 2013						
Associated	Mean	Median		**Non-Associated**	Mean	Median
BAZ	117.04	69.90		BAZ	194.83	231.40
Velocity	3.73	3.70		Velocity	3.59	3.56
Rel. Power (F-K)	0.84	0.88		Rel. Power (F-K)	0.64	0.65
Dominant period	23.14	21.15		Dominant Period	18.41	17.15
SNR	7.6	6.1		SNR	5.3	4.9

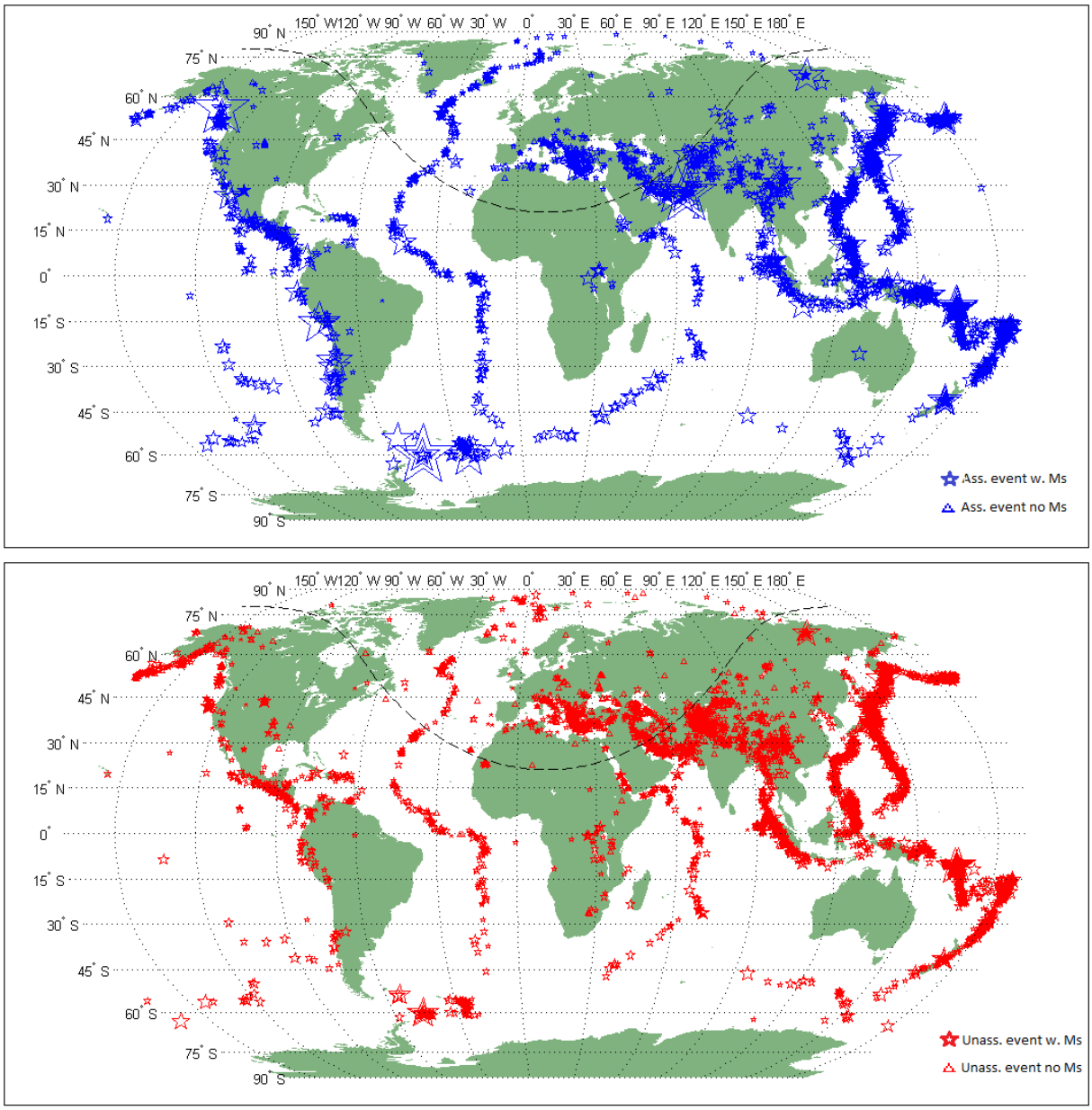

Fig. 6.2.17 World maps of the events listed selected as "detectable" in the association processing for the year 2013. Top plot displays the events with potential Rayleigh waves detected by the NOA DPEP LP detector, while bottom plots the undetected ones. In both plots events with an assigned Ms value are marked by a star, with its size being proportional to the event magnitude. Events with no Ms value in the REBs are displayed as triangles. The black dashed line defines a radius of 40° around NOA.

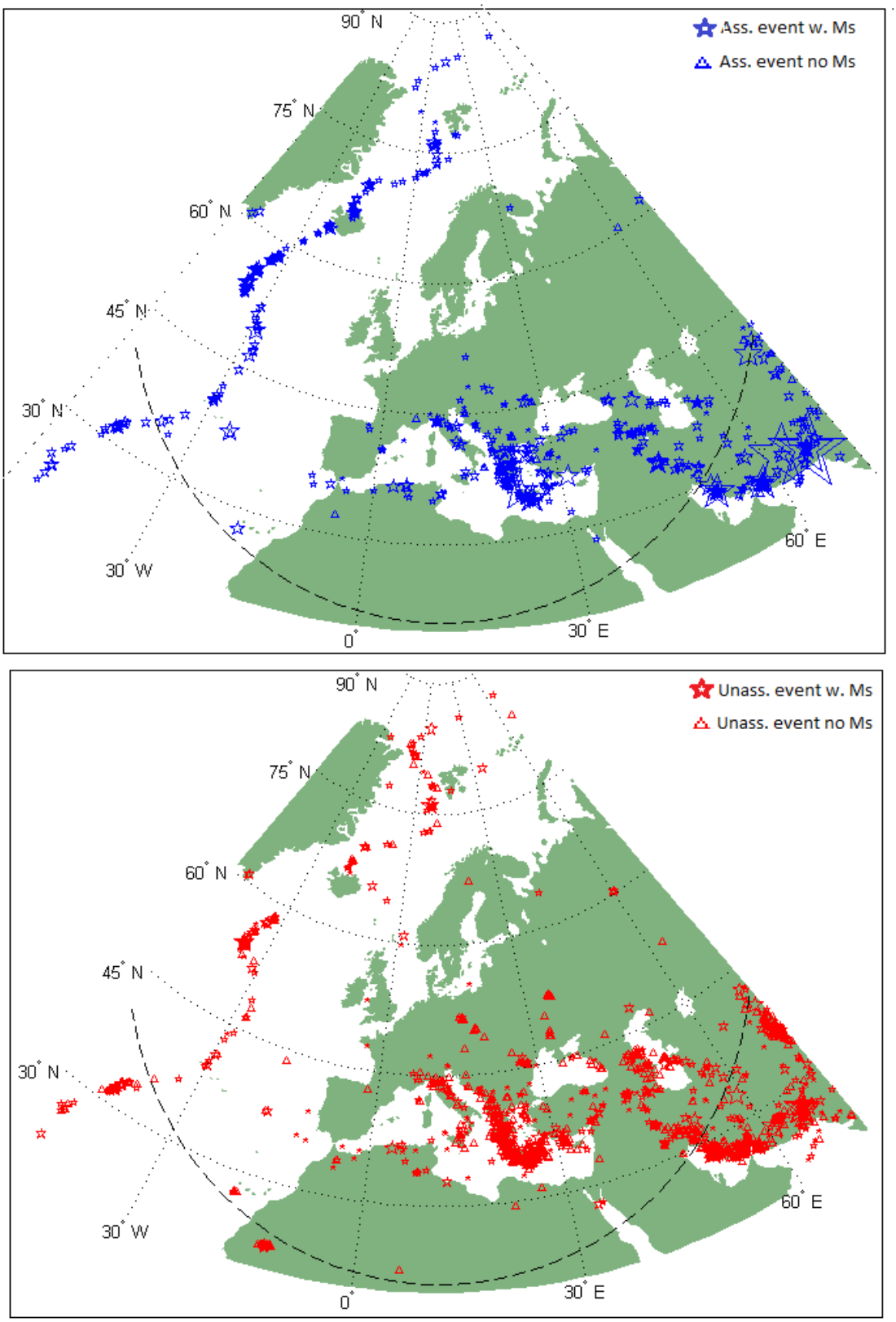

Fig. 6.2.18 European maps displaying the same data of Figure 6.2.17. The black dashed line defines a radius of 40° around NOA.

6.2.5 Conclusions

The NOA DPEP long-period detector achieved promising results in Rayleigh-wave signal detection and recognition. It detects potential surface-wave arrivals down to very low SNR, evaluates their BAZ, velocity, period and amplitude with very high resolution, and in many cases correctly separates body waves from LR detections.

Because of the Rayleigh-type nature of ocean microseisms, it has proven difficult to consistently separate microseism detections from surface waves produced by earthquakes or explosions. The development of a further processing step involving dispersion testing or pattern recognition in near-real time could remedy this shortcoming and potentially yield a powerful tool for surface waves analysis in the CTBT context. Furthermore, such a development could provide very useful information for seismic noise studies, e.g., ambient noise seismic tomography.

Acknowledgements

Most of the presented work was done during research visits of N.L.C. at NORSAR financed by the EC ERASMUS program and the EC research project NERA (#262330). The results were also used as part of the Master thesis of N.L.C. at the University of Trieste.

N. L. Celli, University of Trieste
J. Schweitzer
J. Fyen

References

Bungum, H., S. Mykkeltveit and T. Kværna, 1985, Seismic noise in Fennoscandia, with emphasis on high frequencies, *Bull. Seism. Soc. Amer*., 75, (6), 1489-1513.

Fyen, J. (1987): Improvements and modifications. Semiann. Tech. Summary., 1 Oct 1986 - 31 Mar 1987, *NORSAR Sci. Rep. No. 2-86/87*, Kjeller, Norway. (DP)

Fyen, J. (1989): Event processing program package. Semiannual Tech. Summary, 1 Oct 1988 - 31 March 1989, *NORSAR Sci. Rep. No. 2-88/89*, Kjeller, Norway. (DPEP)

Köhler, A., C. Weidle and V. Maupin, 2011, Directionality analysis and Rayleigh wave tomography of ambient seismic noise in southern Norway, *Geophys. J. Int*., 184, (1), 287–300.

Köhler, A., C. Weidle and V. Maupin, 2012, Crustal and uppermost mantle structure of southern Norway: results from surface wave analysis of ambient seismic noise and earthquake data, *Geophys. J. Int*., 191, 1441–1456.

Kværna T., and D. J. Doornbos, 1986, An integrated approach to slowness analysis with arrays and three-component stations, *NORSAR Sci. Rep*., 2-85/86, 60-69.

Haubrich, A., W. H. Munk and F. E. Snodgrass, 1963, Comparative Spectra of Microseisms and Swell, *Bull. Seism. Soc. Amer*., 53, (1), 27-37.

Longuet-Higgins, M.S., 1950, A Theory of the Origin of Microseisms, *Phil. Trans. R. Soc. London*, Series A, Mathematical and Physical Sciences, 243, (857), 1-35.

Mykkeltveit, S. and H. Bungum, 1984, Processing of regional seismic events using data from small aperture arrays, *Bull. Seism. Soc. Amer*., 74, (6), 2313-2333.

Schweitzer, J., J. Fyen, S. Mykkeltveit, S. Gibbons, M. Pirli, D. Kühn and T. Kværna, 2011, Seismic Arrays, in: IASPEI New Manual of Seismic Observatory Practice, Chapter 9, 80 pp.

Stevens J. and K. McLaughlin, 2001, Optimization of Surface Wave identification and Measurement, *Pure Appl. Geophys*., 158, 1547-1582.

Trnkoczy, A., 1999, Understanding and parameter setting of STA/LTA trigger algorithm, in: IASPEI New Manual of Seismic Observatory Practice, Information Sheet 8.1, 19 pp.